The Journal of Neuroscience, November 1994, 14(11): 6815–6824

N-Type Ca^{2+} Channels Are Located on Somata, Dendrites, and a Subpopulation of Dendritic Spines on Live Hippocampal Pyramidal Neurons

Linda R. Mills,[1,2] Charles E. Niesen,[1] Austin P. So,[1,2] Peter L. Carlen,[1,2] Igor Spigelman,[4] and Owen T. Jones[1,3]

[1]Playfair Neuroscience Unit, Toronto Hospital Research Institute, Toronto Western Hospital, Toronto, Ontario, Canada M5T 2S8, Departments of [2]Physiology and [3]Pharmacology, University of Toronto, Toronto, Ontario, Canada M5S 1A8, and [4]UCLA School of Dentistry and Brain Research Institute, University of California, Los Angeles, Los Angeles, California 90024-1668.

In the nervous system the influx of Ca^{2+} orchestrates multiple biochemical and electrical events essential for development and function. A major route for Ca^{2+} entry is through voltage-dependent calcium channels (VDCCs). It is becoming increasingly clear that the precise contribution VDCCs make to neuronal function depends not only upon their specific electrophysiological properties but also on their distribution over the nerve cell surface.

One location where the presence of VDCCs may be critical is the dendritic spine, a structure known to be the major site of excitatory synaptic input. On spines, VDCCs are hypothesized to play an essential role in signal processing, learning, and memory. However, direct evidence for the presence of VDCCs on spines is lacking. Attempts to examine the distribution of VDCCs, or indeed any other components, on spines have been hampered since the size of many spines is close to the limits of resolution of conventional light microscopy.

Using a new, biologically active, fluorescein conjugate of ω-conotoxin (Fl-ω-CgTx), a selective blocker of N-type VDCCs, and confocal microscopy, we have mapped the distributions of N-type VDCCs on live CA1 neurons in rat hippocampal slices. VDCCs were found on somata, throughout the dendritic arbor, and on dendritic spines in all hippocampal subfields. A comparison of three-dimensional reconstructions of structures labeled by Fl-ω-CgTx with those outlined by 1,1-dioctadecyl-3,3,3′,3′-tetramethylindocarbocyanine (DiI) or Lucifer yellow confirmed the presence of N-type VDCCs on dendritic spines. However, spine frequency on dendrites labeled with Fl-ω-CgTx was much lower than the spine frequency on dendrites labeled with Lucifer yellow or DiI, suggesting that some spines lack N-type VDCCs. These results offer the first direct evidence for the localization of any voltage-dependent channel on dendritic spines. The presence of N-type VDCCs on dendrites and their spines argues that these channels may participate in the generation of active Ca^{2+} conductances in distal dendrites, and is consistent with a role for spines as specialized compartments for concentrating Ca^{2+}.

[Key words: rat, hippocampus, pyramidal neurons, voltage-dependent calcium channels, dendritic spines, ω-conotoxin]

The targeting of voltage-dependent Ca^{2+} channels (VDCCs) to discrete regions of the cell surface provides neurons with a powerful mechanism for coupling a local influx of Ca^{2+} to diverse biochemical and electrical events. Such events include membrane excitability (Llinás and Sugimori, 1979, 1980), neurotransmitter release (Katz, 1969; Augustine et al., 1987), differential gene expression (Sheng and Greenberg, 1990; Bading et al., 1993), neurite outgrowth (Kater and Mills, 1991), neuronal migration (Komura and Rakic, 1992), and the manifestation of various neurological disorders (Gibson and Peterson, 1987; Choi, 1988).

In the dendritic arbor, the segregation of VDCCs and other channels (Llinás, 1988; Craig et al., 1993) appears to be associated, intimately, with the distribution of specific electrophysiological properties. One site where channel distributions may be critically important is the dendritic spine. Owing to their role as major postsynaptic targets for excitatory innervation, spines are considered to be key elements in neural integration, signal processing, and learning and memory (Wickens, 1988; Grover and Teyler, 1990; Shepherd et al., 1990; Koch and Brown, 1992; Kullmann et al., 1992; Koch and Zador, 1993). Their precise role in these events remains unclear but it has long been assumed, on both theoretical and morphological grounds, that spines attenuate or amplify synaptic input (Hounsgaard and Mittgaard, 1989; Shepherd et al., 1990). However, data from electron microscopic studies (Harris and Stevens, 1989; Harris et al., 1992) suggest that in many cases spine shape may be insufficient to modulate synaptic weight effectively (Koch and Zador, 1993). Consequently, other roles for spines have been proposed. In particular, recent evidence indicates that spines may act to isolate or amplify calcium signals and thus function as biochemical rather than electrical compartments (Holmes,

Received Sept. 20, 1993; revised Apr. 22, 1994; accepted May 11, 1994.

We thank P. S. Pennefather and J. H. Eubanks for critical review of the manuscript, and J. K. S. Stevens for making available the ICAR 80.8 workstation used in the three-dimensional reconstructions. This work was supported by funds from the Medical Research Council of Canada, the Ontario Mental Health Foundation, the Sandoz Gerontological Foundation, the Epilepsy Foundation of America, the Bloorview Epilepsy Program, and the University of Toronto.

Correspondence should be addressed to Dr. Owen T. Jones, Playfair Neuroscience Unit, Mc 11-434, Toronto Hospital Research Institute, Toronto Western Hospital, 399 Bathurst Street, Toronto, Ontario, Canada M5T 2S8.

1990; Guthrie et al., 1991; Muller and Connor, 1991; Koch and Zador, 1993).

Whether spines act as electrical or biochemical compartments, or both, the ability of VDCCs to couple voltage changes to Ca^{2+} influx (Miller, 1992) argues that their presence may be critical to spine function. For example, on spines endowed with VDCCs, even small synaptic inputs could trigger large EPSPs in a passive dendrite (Perkel and Perkel, 1985; Shepherd et al., 1985, 1990). Similarly, the activation of VDCCs on individual spines could trigger, or amplify, the local Ca^{2+} influx thought to mediate those biochemical and structural changes associated with synaptic plasticity (Lynch et al., 1983; Malenka et al., 1988; Konnerth et al., 1992; Kullmann et al., 1992; Miyakawa et al., 1992; Regehr and Tank, 1992). However, direct evidence for the presence of VDCCs on spines has been lacking. Due to their small size (near the limit of resolution of light microscopy), spines have only recently been visualized in living tissues (Guthrie et al., 1991; Muller and Connor, 1991; Hosokawa et al., 1992). Using confocal microscopy and a new fluorescent analog of ω-CgTx, a potent, selective blocker of N-type VDCCs (Olivera et al., 1991; Regan et al., 1991; Sher and Clementi, 1991; Mintz et al., 1992), we have mapped the distribution of N-type VDCCs on live hippocampal neurons and provide the first evidence for the localization of VDCCs on dendritic spines. A comparison of Fl-ω-CgTx–labeled neurons to neurons stained with Lucifer yellow or DiI showed that not all spines contained detectable N-type VDCCs. The presence of N-type VDCCs on spines is consistent with a role for spines as either amplifiers of synaptic input or as specialized compartments for concentrating Ca^{2+} (Andrews et al., 1988; Holmes, 1990; Guthrie et al., 1991; Muller and Connor, 1991).

Materials and Methods

Preparation and purification of fluorescein conjugates of ω-conotoxin (ω-CgTx). Fluorescein (Fl)-ω-CgTx was prepared by reacting native ω-CgTx for 10 min at 25°C with the succinimidyl ester of 5(6)carboxyfluorescein (Molecular Probes) (Jones et al., 1989) at a label to toxin ratio of 2:1 mol/mol in 100 mM $NaHCO_3$/24% DMSO (pH 9.5). The reaction mixture was then quenched with 0.5 M glycine and applied to a TSK SP-5PW cation exchange HPLC column. Products were eluted with a linear gradient (1%/min) of 1 M NH_4OAc in 1% HOAc (pH 3.0) and detected by continuous monitoring of the absorbance at 280 nm.

Radiolabeled binding assays. Native ω-CgTx or HPLC-purified conjugates were incubated with rat brain synaptic membranes (0.1 mg/ml protein in 125 μl of 5 mM HEPES-Tris, pH 7.4, 0.1 M sucrose, 0.1% BSA) for 30 min, after which ^{125}I-ω-CgTx (0.3 nM) was added. After 30 min, free and membrane-bound ^{125}I-ω-CgTx were separated by filtration and washing (3 × 2.5 ml wash buffer: 160 mM choline chloride, 5 mM HEPES-Tris, 1.2 mM $CaCl_2$, 0.1% BSA), and filter-bound ^{125}I-ω-CgTx determined by counting gamma emission.

Electrophysiology. Transverse hippocampal slices from 3–6-week-old male Wistar rats were sectioned at 400 μm in ice-cold artificial cerebrospinal fluid (ACSF) solution (in mM): 124 NaCl, 26 $NaHCO_3$, 3 KCl, 1.25 Na_2HPO_4, 2 $CaCl_2$, 2 $MgCl_2$, and 10 D-glucose. Slices were incubated in ACSF bubbled with 95% O_2/5% CO_2 for 1 hr at room temperature prior to recording. Tight-seal, whole-cell patch recordings were made using an Axoclamp 2A amplifier (6–8 kHz sampling rate, 1–3 kHz low-pass filter) and pCLAMP software (Axon Instruments). Electrode tip resistances were 3–5 MΩ. The extracellular voltage-clamp solution contained (in mM) 130 NaCl, 3 KCl, 4 $CaCl_2$, 2 $MgCl_2$, 26 $NaHCO_3$, 10 D-glucose, 30 TEA, 3 $CsCl_2$, 5 4-AP, and 0.5 μM TTX (pH 7.4). The recording pipette solution contained (in mM) 150 Cs-gluconate, 35 CsOH, 10 BAPTA, 10 HEPES, 0.1 $CaCl_2$, 2 Mg-ATP, 25 phosphocreatine, 50 U of phosphocreatine kinase, and 100 μM leupeptin adjusted to pH 7.25–7.30 with HCl; solutions ranged from 285 to 300 mOsm. Calcium currents showed little rundown and were stable for >40 min. Native and Fl-ω-CgTx were applied with a puffer microelectrode using a picospritzer. Bath perfusion of ω-CgTx at concentrations used for imaging (0.5–1 μM) gave similar levels of block as Fl-ω-CgTx. Synaptic potentials were evoked with a concentric stimulating electrode in the stratum radiatum (0.1 msec, 10–100 μA at 30 sec intervals). For current-clamp recordings, microelectrodes contained (in mM) 150 K-gluconate, 4 KCl, 10 HEPES, 2 Mg-ATP, 0.1 $CaCl_2$, 1 BAPTA, and 0.2 GTP. Bicuculline (10–20 μM in ACSF) was used to block inhibitory postsynaptic potentials. Four or five EPSP responses were averaged before and after toxin application. All recordings were made at room temperature.

Labeling of N-type VDCCs on hippocampal neurons with Fl-ω-CgTx. Live hippocampal slices were sectioned at 200–250 μm, as for electrophysiology. Individual sections were incubated for 30–45 min with 1.0 μM ω-CgTx, or 0.5–1.0 μM Fl-ω-CgTx in either ACSF bubbled with 95% O_2/5% CO_2, at room temperature, or modified Eagle's medium (MEM) at 37°C in 5% CO_2. Slices were then rinsed in ACSF or MEM, transferred to glass-bottomed dishes in a temperature controller unit, and viewed immediately in HEPES-buffered MEM. In some cases labeled slices were rinsed and fixed overnight in 4% paraformaldehyde. The fixed slices were subsequently dehydrated, and cleared in methylsalicylate or mounted in Mowiol to reduce photobleaching.

Intracellular labeling with Lucifer yellow. Single pyramidal neurons in the CA1 region were filled by injection via patch electrodes with the intracellular dye Lucifer yellow at a concentration of 0.1% in ACSF, and fixed overnight with 4% paraformaldehyde in 0.1 M phosphate buffer, rinsed, dehydrated in alcohol, and cleared with methyl salicylate, or mounted in Mowiol.

Labeling of neurons with DiI. Neurons in CA1, CA2, and CA3 were labeled by incubating slices in DiI (10 μg/ml) (Molecular Probes) in ACSF or MEM for 30–90 min. The slices were then rinsed and either viewed immediately, or fixed as above prior to viewing.

Confocal microscopy. Slices labeled with Fl-ω-CgTx were viewed with an inverted scanning confocal microscope (Bio-Rad MRC-600) equipped with an argon-ion laser (ILT), using the fluorescein filter set and either fluor (10× and 20×) or planapo (60×) objectives. Emitted fluorescence was displayed through the framestore of the host computer. An adjustable pinhole in the detector lightpath controlled the optical section thickness, and illumination intensity was controlled by the use of a filter wheel. Typically, single confocal images used for spine counts (see below) were collected with the pinhole aperture stopped down. This procedure reduces the thickness of the optical section so that fewer dendritic segments are imaged; other labeled dendritic segments (numerous in preparations labeled with Fl-ω-CgTx or DiI) just above or below the focal plane are eliminated. Preliminary experiments indicated that Fl-ω-CgTx–labeled preparations were subject to photobleaching, and a neutral density filter of 1 was used on all preparations (except when otherwise indicated; see Results). All optical series were taken using a single scan per section. Dendritic segments were optically sectioned relative to their longitudinal axis using step sizes (the distance between two optical sections) of 0.3 μm. Since photobleaching increases as the number of sections in the data set increases (Stevens et al., 1990; Rigaut and Vassy, 1991), only dendritic segments running more or less perpendicular to the z-axis (which minimizes the number of sections required) were selected for optical sectioning. Similar conditions were used to collect data from fixed Lucifer yellow–, and live and fixed DiI-labeled preparations. Lucifer yellow–labeled CA1 neurons were viewed using the fluorescein filter set, and DiI-labeled neurons were viewed using the rhodamine filter block.

Determination of spine frequency and spine length on dendrites of CA1 pyramidal neurons. Spine frequencies in neurons labeled with Fl-ω-CgTx, DiI, or Lucifer yellow were determined by counting spines on 20 dendritic segments (DS) from each of the five preparations examined. (These five preparations were live and fixed neurons labeled with Fl-ω-CgTx, live and fixed neurons labeled with DiI, and fixed neurons labeled with Lucifer yellow.) The criteria for selecting the dendritic segments were as follows. All segments were from apical dendrites within 25–80 μm of the somata in CA1, 7–29 μm long, and contained at least two spines. Structures were identified as spines only if they were >0.43 μm long and continuous with the parent dendrite. Spine counts were determined by counting all visible spines in a single image of a selected DS; however, in some cases an adjacent serial section was viewed to confirm continuity, that is, the presence of a spine shaft, between putative spine heads and the parent dendrite. Reported spine frequencies are the average number of spines on the 20 DS in each preparation ± SEM. To eliminate bias in estimates of spine frequency, approximately 25% of all samples (four or five from each preparation), chosen at random, were examined by blind observers. Since estimates of spine frequency appeared to be independent of prior observer knowledge of the experimental conditions, blind and nonblind data were pooled.

Spine frequencies were also determined using three-dimensional re-

constructions of serial confocal data sets from Fl-ω-CgTx–, DiI-, and Lucifer yellow–labeled preparations. Such reconstructions, while time consuming to generate, provide more accurate counts of total spine numbers than can be achieved using one or even two single images. By rotating the reconstructions spines can be readily counted on all surfaces of the dendrite; in contrast, spine counts from single images will exclude spines above or below the plane of focus. Six DS from each preparation were selected according to the criteria described above and optically sectioned as previously described. These data sets were then reconstructed on a Volume Investigation workstation (see below), and spines were counted on all surfaces of the three-dimensional image.

The range of spine lengths in each preparation was determined using the dendrites selected for spine frequency counts. Spine and dendritic lengths were determined using Bio-Rad or ICAR software. Selected DS from more distal sites in CA1 (70–150 μm from cell somata in CA1), and DS from areas CA2, CA3, and DG were also examined for the presence of spines, but spine lengths and frequencies were not determined in these preparations.

Three-dimensional reconstructions of confocal data. Three-dimensional reconstructions of serial confocal data sets were carried out on a UNIX-based ICAR 80.8 Volume Investigation workstation (ISG Technologies, Mississauga, ON). The workstation uses an 80 MIP parallel graphics processor to convert two-dimensional pixels from the original confocal images into units of volume or three-dimensional voxels. Reconstructions were based on segmentation of the gray-scale image data stack using simple thresholds. Selected density ranges were chosen using histograms of the entire image stack, and peaks selected represented maximum pixel intensities. Details have been described elsewhere (Stevens et al., 1990; Harris et al., 1992; Mills and Nurse, 1993; Mills, 1994; Mills et al., 1994).

Results

Purification and characterization of fluoresceinated ω-conotoxin

Acylation of synthetic ω-CgTx with the succinimidyl ester of 5(6)carboxyfluorescein under lysine-modifying conditions yields multiple reaction products, free dye, and unreacted ω-CgTx. Despite its complexity, this mixture can be readily resolved by ion-exchange high-performance liquid chromatography (Fig. 1*A*), using a gradient of ammonium acetate in water as eluent. The purity of selected peaks was then confirmed by reverse-phase HPLC. To identify potentially active ω-CgTx conjugates, each HPLC fraction was screened for its ability to displace ^{125}I-ω-CgTx from brain membranes at equivalent toxin concentrations (Fig. 1*A*, inset). The potency of the most active fractions (peaks a, b, and c) was then compared to that of unmodified ω-CgTx from their ability to displace ^{125}I-ω-CgTx from rat brain membranes in a concentration-dependent manner (Fig. 1*B*). The apparent dissociation constants ($K_{d,app}$) for the three most potent conjugates (peaks a, b, and c) were 7, 22, and 2 nM, respectively, while the $K_{d,app}$ for ω-CgTx (*) was 40 pM.

Electrophysiology

In whole-cell recordings from CA1 neurons in rat hippocampal brain slices, ω-CgTx and the Fl-ω-CgTx analog (fraction a) reduced the high-threshold Ca^{2+} current evoked from a hyperpolarized holding potential (−65 to −80 mV) by 34.3 ± 4.1% (±SEM; n = 4) and 30.2 ± 4.0% (±SEM; n = 5), respectively, when focally applied at 10 μM. The magnitude of this block was similar to that observed previously with saturating concentrations of ω-CgTx in dissociated CA1 neurons (Regan et al., 1991). Blockade by Fl-ω-CgTx had a rapid onset ($t_{1/2}$ < 15 sec) and usually did not wash out after >20 min. Stimulation of the Schaffer collateral pathway produced excitatory postsynaptic potentials (EPSPs) in CA1 neurons that were decreased by 21.8 ± 3.6% (±SEM; n = 5) after 10 μM ω-CgTx droplet application (Fig. 2*C*). Additional applications of ω-CgTx produced no further block of EPSPs and single postsynaptic spikes were readily elicited from larger EPSPs with higher stimulus strengths (Horne and Kemp, 1991).

Visualization of N-type VDCCs on hippocampal pyramidal neurons

The distribution of VDCCs on living adult rat hippocampal neurons was visualized by laser confocal microscopy of brain slices labeled with Fl-ω-CgTx (Fig. 2). Intense labeling of N-type channels was seen on somata and dendrites in all hippocampal regions (Fig. 2*A*). Strong labeling was also seen in the entorhinal cortex and on putative interneurons in the hilar region of the dentate gyrus. Staining was absent on axons and glia or in controls made by pretreating slices with ω-CgTx (Fig. 2*B*).

Labeling by Fl-ω-CgTx of apical dendrites extended from the soma for at least 280 μm. The labeling intensity varied on dendrites (and somata) (Fig. 2*C–F*). Serial optical sectioning confirmed that this unevenness in intensity was due to local differences in VDCC density rather than undulations of the cell surface in and out of the plane of focus. Thus, in regions where Fl-ω-CgTx labeling was low, the fluorescence intensity did not increase on stepping to adjacent in-focus serial sections. In contrast, the in-focus fluorescence intensity was constant in optical sections taken from neurons with surfaces defined by DiI or Lucifer yellow.

Numerous small structures projecting from the dendritic shafts were observed in all subfields and identified as dendritic spines based on morphological criteria. However, only those spines on apical dendrites within a defined region of CA1 (see Materials and Methods) were examined in detail. Structures defined by Fl-ω-CgTx in live CA1 dendrites (Figs. 2*C*(arrows),*D–F*; 3*A*) were 0.5–2.1 μm long (n = 123 spines), consistent with spine lengths measured on dendrites from live CA1 neurons outlined with DiI (Fig. 3*B*) (0.5–2.1 μm; n = 525). Spines observed in living neurons labeled with Fl-ω-CgTx or DiI were comparable in length to their counterparts in fixed CA1 neurons (0.5–1.9 μm, n = 106 spines; 0.43–2.2 μm, n = 418 spines, respectively), or in neurons filled with Lucifer yellow (0.5–2.0 μm; n = 625). In all preparations spines were not detected adjacent to the cell bodies (within 10 μm), consistent with the known distributions of spines in CA1 neurons (Harris and Stevens, 1989). Viewing conditions produced no detectable distortion of dendrites and spines in live slices examined up to 2 hr after labeling (see, e.g., Fig. 3*A,B*); however, considerable swelling of cell bodies, dendrites, and spines was apparent in some preparations after periods greater than 3 hr. Such preparations were discarded.

In many cases, uninterrupted Fl-ω-CgTx labeling between the spine head and parent dendrite could be observed in a single image (Figs. 2, 3). In other cases, adjacent serial sections were necessary to confirm the identity of labeled structures; only those attached to the parent dendrite were classified as spines. In living slices labeled with Fl-ω-CgTx (Figs. 2*C–F*, 3*A*), spines of varying size projected intermittently along dendritic shafts at a frequency of 0.34 ± 0.02 spines/μm (±SEM; n = 20 DS). In contrast, the spine frequency in live slices labeled with DiI (see Fig. 3*B*) was significantly higher, 1.24 ± 0.08 spines/μm (±SEM; n = 20 DS) (p < 0.001, Fl-ω-CgTx vs DiI, two-tailed t test). In fixed preparations, spine frequencies were also significantly lower in Fl-ω-CgTx–labeled preparations, 0.41 ± 0.08 spines/μm (±SEM; n = 20 DS), compared to DiI-labeled preparations, 1.46 ± 0.06 spines/μm (±SEM; n = 20 DS), or Lucifer yellow–filled neurons, 1.36 ± 0.11 spines/μm (±SEM; n = 20 DS) (p < 0.001, Fl-ω-CgTx vs Lucifer yellow, and p < 0.001, Fl-ω-CgTx vs DiI, two-tailed t test). The frequency of spines in Fl-

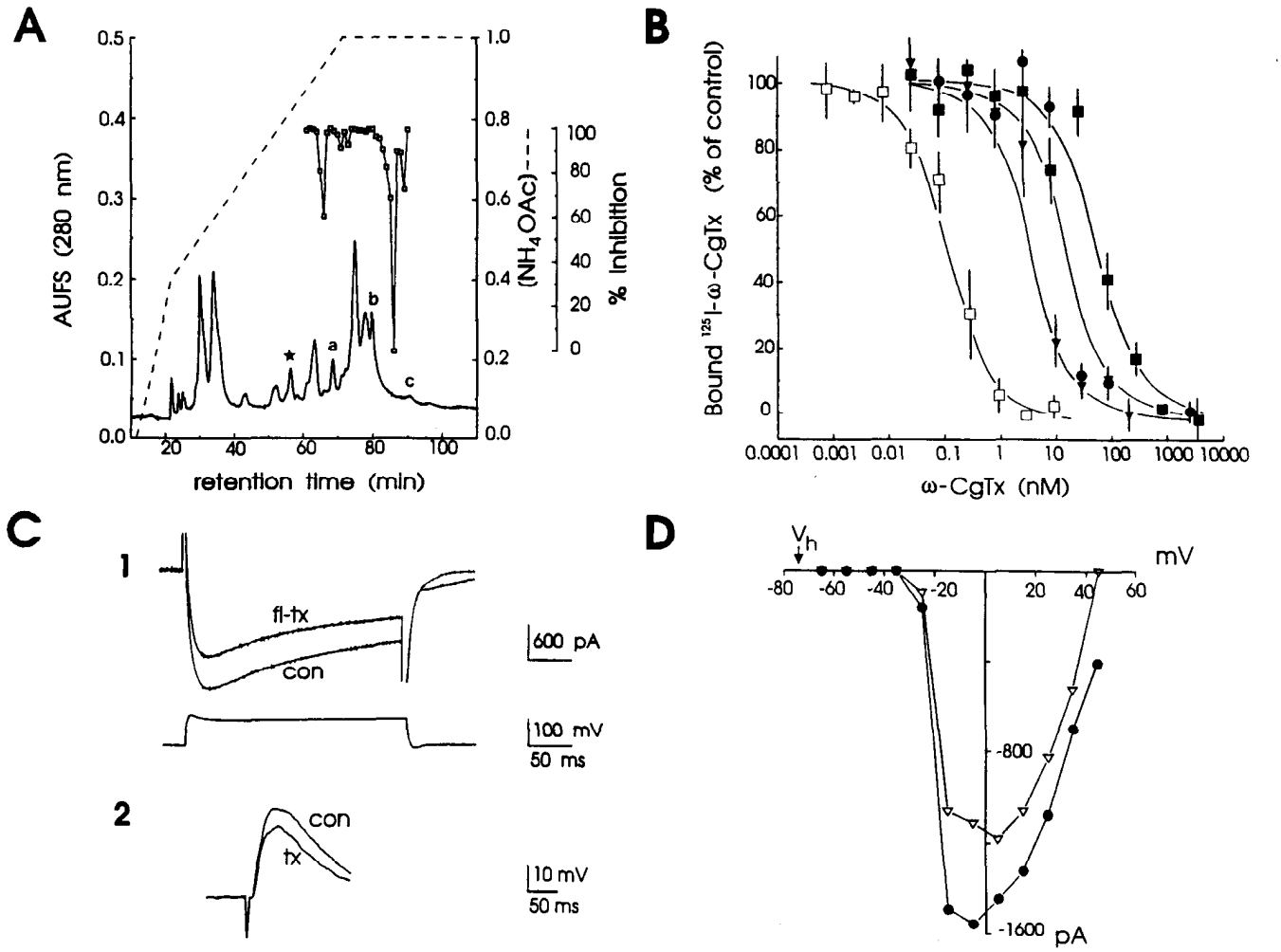

Figure 1. Purification and characterization of ω-conotoxin (ω-CgTx) analogs and their effect on the high-threshold Ca^{2+} current and EPSPs in hippocampal CA1 neurons. *A*, Resolution of ω-CgTx, Fl-ω-CgTx, and free dye products by ion exchange HPLC. *B*, Displacement of ^{125}I-ω-CgTx from rat brain synaptic membranes by ω-CgTx (□), and peaks *a* (●), *b* (■), and *c* (▼). Values represent mean ± SD (n = 9). *C*, Inhibition of the high-threshold Ca^{2+} current and synaptic potentials in CA1 neurons. *C1: Top trace,* High-threshold Ca^{2+} current elicited on a voltage step to −5 mV (*con*) from a holding potential of −75 mV was decreased by 31% after focal application of 10 μM Fl-ω-CgTx (*fl-tx*). Capacitive currents were clipped to fit the figure. *Bottom trace,* The 70 mV step that evoked the Ca^{2+} current. *C2,* The averaged responses of four EPSPs before (*con*) and after (*tx*) 10 μM ω-CgTx was applied to the apical dendrites and somatic region of a different CA1 neuron. Stimulus artifact is evident before the depolarization. Resting membrane potential was −65 mV. *D,* The peak current–voltage relation of the high-threshold Ca^{2+} current before (●) and after (▽) addition of 10 μM Fl-ω-CgTx, same cell as in *C1*. In *C1*, depolarizing voltage steps (200 msec duration) were applied in 10 mV increments from a membrane holding potential of −75 mV.

ω-CgTx–treated preparations did not increase significantly with prolonged incubations or increased concentrations of label. Two dendrites labeled with Fl-ω-CgTx were imaged twice, once with a neutral density filter present and once after the filter was removed. The number of spines visible was not different in these images, indicating that the use of ND filters did not mask a subpopulation of weakly labeled spines.

Spine frequencies were also determined using three-dimensional reconstructions of serial confocal data sets from live neurons labeled with Fl-ω-CgTx or DiI (Fig. 4), or on fixed neurons labeled with Lucifer yellow. This procedure provides a more accurate count of total spine numbers since spines above or below the plane of focus of a single image are included in the multiple image stack used in the reconstruction. In addition, the distribution of spines on all dendritic surfaces is more readily appreciated in the three-dimensional reconstructions. Overall dendritic morphology and spine lengths were similar in reconstructions of live neurons from preparations labeled with Fl-ω-CgTx, DiI (Fig. 4), or fixed neurons labeled with Lucifer yellow. Spine frequency, however, was markedly lower in reconstructions of Fl-ω-CgTx–labeled living dendrites (0.48 ± 0.07 spines/μm; n = 6 reconstructions), compared to spine frequency in reconstructions of DiI-labeled living dendrites (2.21 ± 0.19 spines/μm; n= 6 reconstructions) or fixed Lucifer yellow–labeled dendrites (2.01 ± 0.15 spines/μm; n = 6 reconstructions).

Discussion

These data provide direct evidence for the localization of N-type VDCCs on the somata and dendrites of live hippocampal neurons and are the first demonstration that VDCCs exist on spines. The somatodendritic staining pattern is consistent with previous studies using autoradiography (Kerr et al., 1988; Takemura et

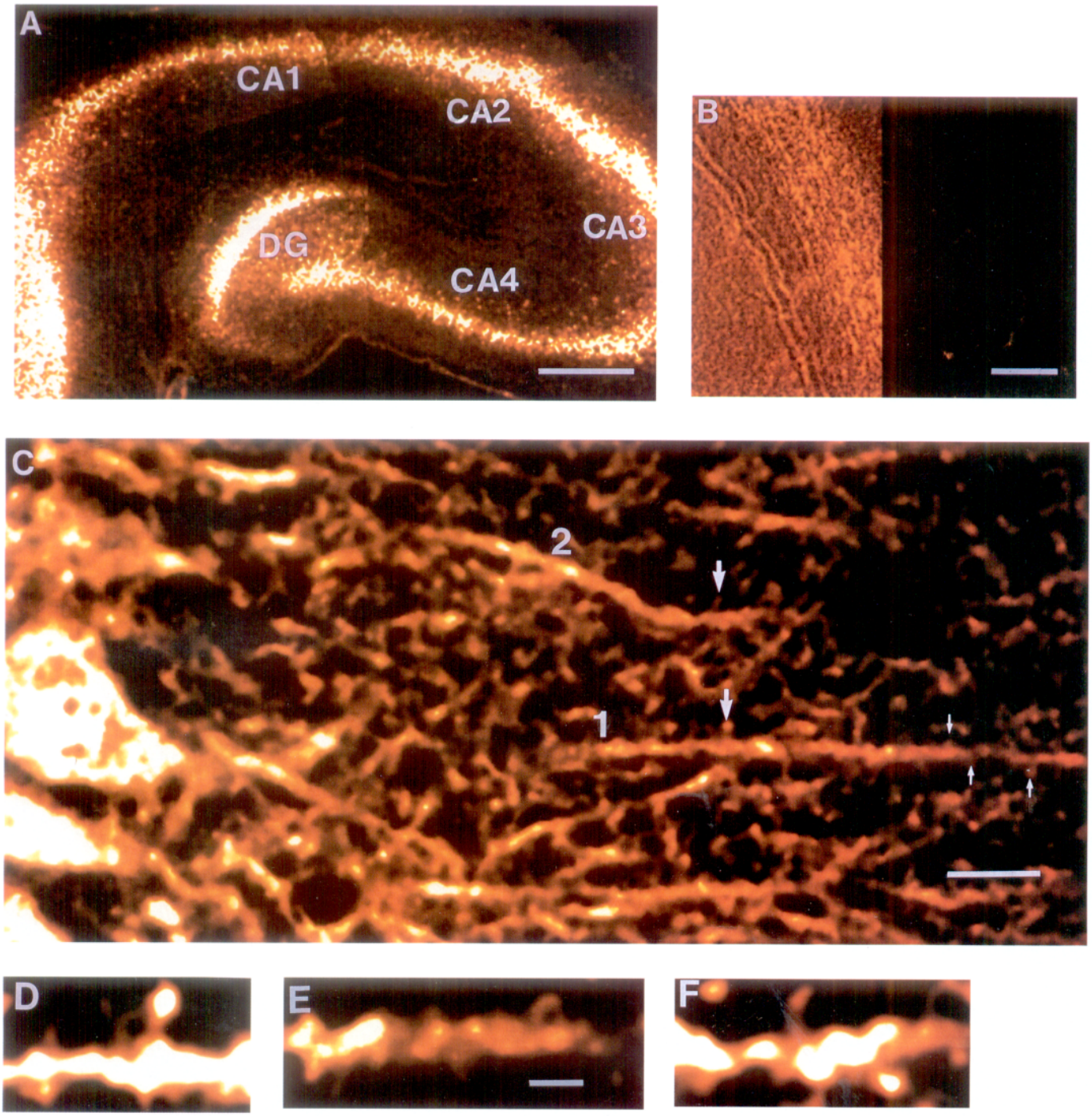

Figure 2. Distribution of N-type VDCCs in living hippocampal pyramidal neurons and interneurons visualized by confocal microscopy. *A,* Overall view of a transverse hippocampal slice labeled with Fl-ω-CgTx. *B,* Control section labeled with ω-CgTx (1 μM) prior to incubation with Fl-ω-CgTx. *Right,* fluorescence; *left,* transmitted light. *C,* At 60×, intensely labeled somata in CA1 (*far left*) and multiple dendrites (see, e.g., those labeled *1* and *2*) are visible. Individual spines, some of which are marked with *arrows,* are visible along many dendrites. *D,* Enlargement of an individual spine projecting from dendrite *1* (indicated by a *large arrow* in *C*) showing details of spine head and neck. *E,* Enlargement of other spines of various sizes on the same dendrite (labeled with *small arrows* in *C* on dendrite 1). *F,* Enlargement of spines on dendrite 2 (from area marked by *large arrow* in *C*). Scale bars: *A,* 375 μm; *B,* 20 μm; *C,* 5 μm; *D–F,* 2 μm.

al., 1988), electrophysiology (Blaxter et al., 1989; Fisher et al., 1990), or labeling of CA1 neurons in culture (Jones et al., 1989), but differs from the largely dendritic labeling seen with CNB-1, an antibody to a subtype of N-type VDCCs (Westenbroek et al., 1992). Since Fl-ω-CgTx labels all N-type VDCCs, the lack of somatic labeling observed with CNB-1 suggests that subtypes of N-channels exist that are restricted to specific neuronal compartments. The uneven labeling seen along dendrites supports the existence of hot spots of Ca^{2+} influx (Lipscombe et al., 1988; Jones et al., 1989; Silver et al., 1990; Westenbroek et al., 1992), but unlike on Purkinje cells (Westenbroek et al., 1992) these hot spots were not consistently found at dendritic branch points. The presence of N-type VDCCs on distal dendrites implicates this class of channel in the generation of dendritic Ca^{2+} spikes

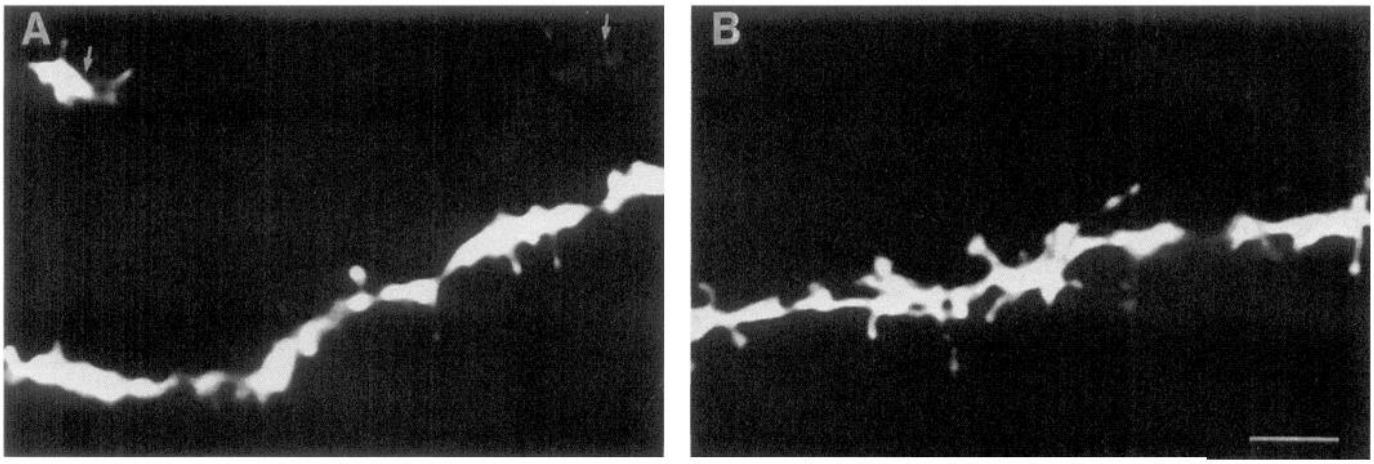

Figure 3. Single confocal images of dendrites and spines on live CA1 hippocampal neurons. *A,* Apical dendrite segments labeled with Fl-ω-CgTx. Three dendritic segments are visible; however, only one of the three is both in focus and long enough to be used for spine counts. The other two are either out of focus and barely visible (*top right*), or too short (*top left*). *B,* Single dendritic segment labeled with DiI, from a similar region 60 μm from the somata in CA1. In both *A* and *B* the pinhole on the confocal was stopped down to reduce the thickness of the optical section (see text) and improve visualization of spines. Background fluorescence was subtracted and the images were digitally enhanced with a 3 × 3 median filter. Scale bar, 4 μm.

(Schwartzkroin and Slawsky, 1977; Wong et al., 1979; Shepherd and Woolf, 1990; Wong and Stewart, 1992). Dendritic N-type VDCCs can also explain other phenomena such as the improved efficacy of distal synapses (Andersen et al., 1980; Andersen, 1986) and the nonuniform distribution of active dendritic membrane properties (Llinás and Sugimori, 1979).

In previous studies on amphibian synapses, we and others have demonstrated an extensive presynaptic localization of

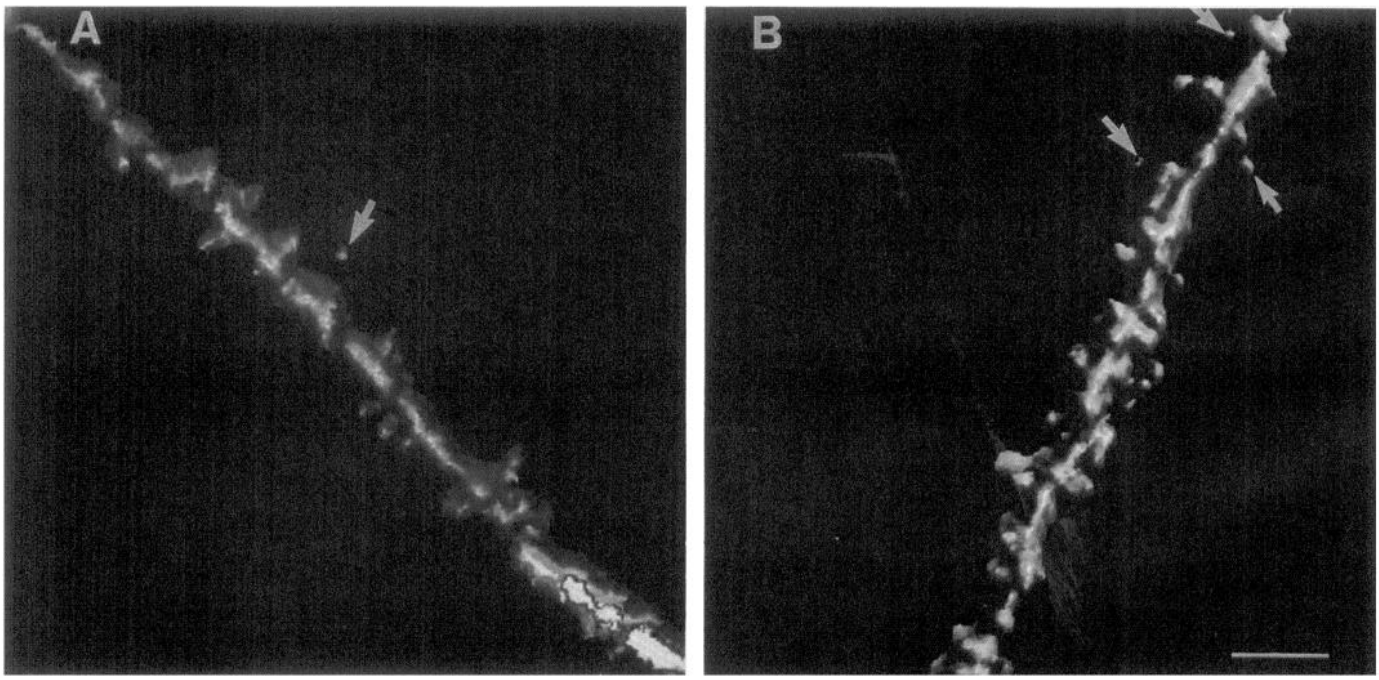

Figure 4. Three-dimensional reconstructions of serial confocal data sets of apical dendritic segments from live hippocampal neurons in CA1. Dendritic segments labeled with Fl-ω-CgTx or DiI were optically sectioned and reconstructed as described in the text. Both reconstructions were done using a 12 slice image stack. *A,* Reconstruction of a living Fl-ω-CgTx–labeled dendrite and its spines. Individual spines are visible projecting from all surfaces of the dendrite visible from this angle. Rotation of the reconstruction revealed other spines on the underside of the dendrite not visible in this image. An isolated structure resembling a spine head is visible halfway along the top edge of the dendrite. Rotation of the image revealed that this structure was unconnected to the dendrite at any point and it may represent a partially labeled spine (lacking labeling along the spine neck), or possibly a labeled presynaptic ending. At the *lower right,* the dendrite appears flattened since this portion of the dendrite was outside the z-axis range of this data set and was therefore only partially optically sectioned. *B,* Reconstruction of a live dendrite labeled with DiI from a similar area in CA1 as in *A.* Spines of various sizes project from all visible surfaces of the dendrite. Three small isolated structures (see *arrows*), putative spine heads, are visible along the dendrite. In this case, inspection of the reconstruction from another angle revealed that all of the "heads" were attached to the dendrite and they were classified as spines. Scale bar, 4 μm.

N-type VDCCs (Robitaille et al., 1990; Cohen et al., 1991). In this study our resolution was such that we could not exclude the possibility that some of the labeling observed was presynaptic. In particular, since the gap between presynaptic and postsynaptic terminals in CA1 neurons is approximately 0.01 μm (Harris and Stevens, 1989; Peters et al., 1991), our optical techniques could not discriminate between presynaptic and postsynaptic labeling on spine heads. Nevertheless, our resolution (~0.21 μm, with 1.4 NA at λ_{ex} of 488 nm) was more than adequate to identify many labeled structures as spines. Since presynaptic innervation occurs almost exclusively at the spine head (Harris and Stevens, 1989; Harris et al., 1992; Koch and Zador, 1993), much of the observed labeling could not be due to VDCCs on presynaptic terminals. A comparison of the observed labeling pattern with that expected for a presynaptic distribution of VDCCs (see Fig. 5) supports this conclusion. Thus, if labeling on spines was exclusively presynaptic, the apical distribution of excitatory presynaptic terminals that occurs on CA1 spines (Harris and Stevens, 1989; Peters et al., 1991) (but not on the dendritic shaft) would generate a roughly parallel array of punctate fluorescence at least 1–2 μm opposite (apparently spineless) parent dendrites (Fig. 5*A*). Instead, patterns of labeling consistent with either Figure 5, *B* or *C*, were observed, consistent with extensive, but not necessarily exclusive, labeling of spines. Indeed, there is good evidence that at central glutamatergic synapses, such as those utilized by spines in CA1 neurons, neurotransmitter release is unaffected by ω-CgTx but is mediated by non–ω-CgTx–sensitive, P-type VDCCs (Turner et al., 1992). These data would preclude presynaptic staining by Fl-ω-CgTx unless N-type VDCCs are present at presynaptic terminals but do not play a role in neurotransmitter release. We hypothesize that the modest effect of ω-CgTx on the EPSP amplitude is due to a blockade of that portion of the depolarization associated with calcium influx through N-type VDCCs in the spine.

The lower spine frequency in Fl-ω-CgTx–labeled neurons compared to spine frequencies determined in neurons labeled with Lucifer yellow or DiI strongly suggests many spines do not have N-type VDCCs. However, an alternative possibility is that some spines with VDCCs might have been undetected. Unlike Lucifer yellow and DiI, the distribution of Fl-ω-CgTx labeling is not homogeneous but rather reflects the distribution of N-type VDCCs; if VDCCs are localized to specific areas of the spine, such as the head, only those regions will be imaged. Since the criteria used to identify spines is based on the presence of labeling contiguous with the dendritic shaft, such partially labeled spines would have been excluded from our spine counts. Consideration of the observed pattern of Fl-ω-CgTx labeling (see Fig. 5) suggests that this explanation is unlikely to account for the approximately 75% of "missing" spines since numerous punctate spots apposed, but unattached, to the dendritic shaft were not observed (as would be expected if many spines were only partially labeled). To resolve the proportion of spines that possess N-type VDCCs unambiguously would require double labeling of both the spines along a dendrite and the VDCCs. In the complex terrain of a slice preparation this approach was not possible due to difficulties in labeling and injecting dye into the same individual neuron. Moreover, such experiments demand the use of pairs of fluorophores with nonoverlapping excitation and emission spectra to eliminate detectable fluorescence bleedthrough. In our system such discrimination was not achievable using a combination of DiI and Fl-ω-CgTx. Although

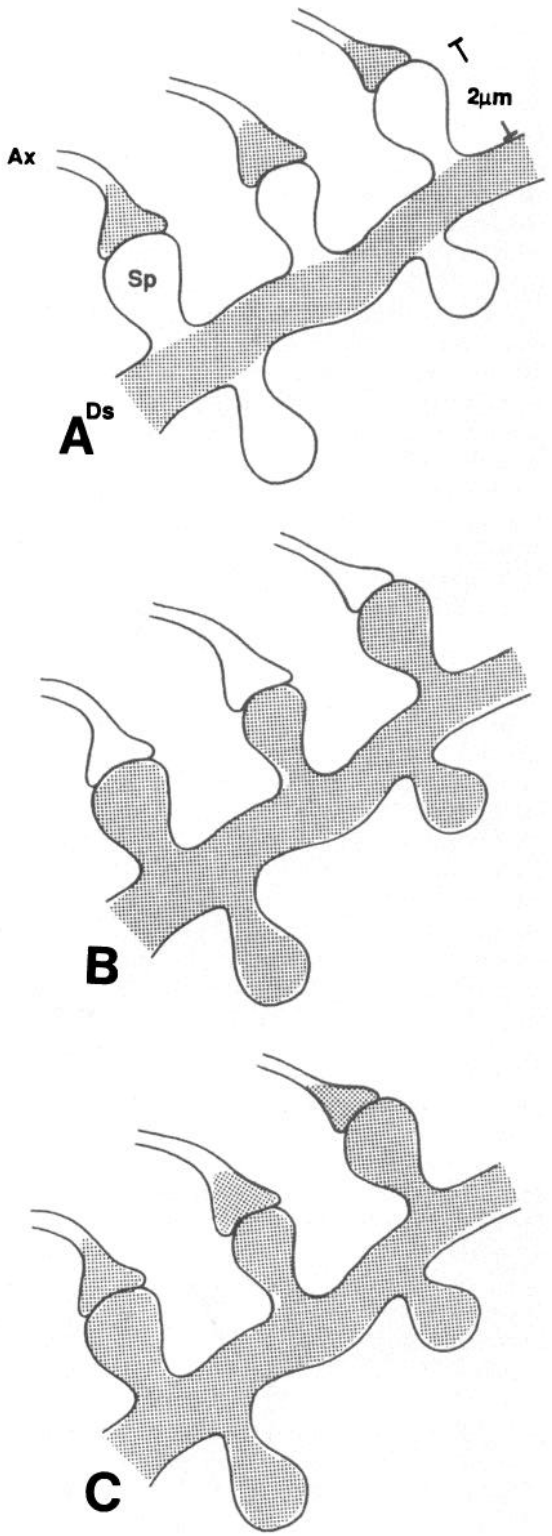

Figure 5. Schematic showing fluorescence staining pattern (*shaded*) predicted for: *A*, Exclusive labeling of VDCCs on presynaptic terminals and dendritic shafts but not spines. *B*, Exclusive postsynaptic labeling of VDCCs on spines and shafts. *C*, Presynaptic labeling of terminals and postsynaptic labeling of VDCCs on the dendritic spine and shaft. Axons, spines, and dendritic shafts are denoted as *Ax*, *Sp*, and *Ds*, respectively.

Fl-ω-CgTx is visible only in the green channel, the DiI signal is visible in both channels (appearing red in one channel, and green-gold in the other), effectively masking any colocalized Fl-ω-CgTx signal.

It should be noted that since extremely thin or small (<0.43 μm in length) spines would have been undetected by our methods, the spine frequencies reported here, using either two- or three-dimensional images, will be an underestimation of the true spine frequencies in all of the preparations we examined. Nevertheless, since our estimates of spine frequency using three-dimensional reconstructions of dendrites labeled with Lucifer yellow or DiI are within the range of those reported in studies using electron microscopy, albeit from areas of CA1 adjacent to those employed here (Harris and Stevens, 1989; Harris et al., 1992), it seems plausible that these small spines do not comprise a major portion of the spine population. Regardless of the contribution such spines make to the true spine population, the finding that *Fl-ω-CgTx labels about 25% of that spine population defined by DiI or Lucifer yellow* argues that N-type VDCCs are present on only a subset of dendritic spines.

The functional implications of a nonuniform distribution of a single class of VDCCs are intriguing. There is good evidence that owing to the Ca^{2+} buffering capacity of the neuron the diffusion of free Ca^{2+} may be very limited, spatially and temporally. In dendrites, the concentration of VDCCs into hot spots could amplify free Ca^{2+} in discrete subcellular compartments, or trigger local calcium-dependent events. Modeling studies suggest that a nonuniform distribution of channels may be more effective at branches than if the channels are distributed evenly over the cell surface (Shepherd et al., 1990). A more subtle argument concerns the possibility that the weighting of synapses thought to underlie learning and memory may involve changes in ion channel structure or function, for example, by posttranslational modification (Bliss and Collingridge, 1993). In such cases the establishment of weighted synapses required for long-term memory would demand the segregation of the modified from the nonmodified channels.

The presence of an asymmetric distribution of VDCCs also has important implications for neuronal cell biology. Since VDCCs are integral membrane proteins (Glossmann and Striessnig, 1990; Witcher et al., 1993), their segregation in the fluid lipid bilayer argues for some restraining mechanism opposing the more energetically favored random VDCC distribution. This is supported by fluorescence photobleach recovery measurements of the lateral mobility of N-type VDCCs in hippocampal neurons (Jones et al., 1989), where at least 80% of VDCCs had a diffusion coefficient of $<10^{-12}$ cm^2sec^{-1} and were thus immobile. How N-type VDCCs may be immobilized is unknown, but the most likely possibility involves tethering to the underlying cytoskeleton. Indeed, such an interaction has been detected between the rat brain voltage-dependent Na^+channel, a protein structurally related to VDCCs (Glossmann and Striessnig, 1990), and the cytoskeletal linker ankyrin (Srinivasan et al., 1988). Attachment of VDCCs to the cytoskeleton could be significant since alterations in the neuronal cytoskeleton are known to occur during activation of NMDA receptors (Seubert et al., 1988), growth cone–target interactions (Lin and Forscher, 1993), and aging (Fifkova and Morales, 1992).

An important question is how VDCCs may be selectively targeted to discrete dendritic spines. In one current model, based on comparisons with polarized epithelia (Rodriguez-Boulan and Powell, 1992), the polarized delivery of neuronal proteins involves sorting to just two discrete domains—the axon and the somatodendrites (Dotti and Simons, 1990). Presumably, such sorting involves recognition of targeting signals lying within the protein, or mRNA structure. Although such a model could readily account for trafficking of VDCCs to somatodendrites, it seems inadequate to explain the targeting of VDCCs to dendritic subdomains (Westenbroek et al., 1990, 1992) or to subpopulations of spines. It is possible a hierarchy of targeting signals encodes specific neuronal locales. Alternatively, VDCCs may be sorted to dendrites and subsequently redistributed to selected spines by the influence of epigenetic factors such as synaptic activity (Craig et al., 1993) or glial contact. Interestingly, the targeting of channels to a subset of dendritic spines appears to extend to another class of ion channels—those gated by glutamate (Craig et al., 1993). In their study, clusters of GluR1 and GluR2/3 were restricted to a subset of postsynaptic sites in hippocampal pyramidal cells in culture. Whether VDCCs and glutamate receptors are targeted to a subset of spines by similar mechanisms, and whether these spines represent the same subpopulation, is as yet unclear.

The targeting of VDCCs to a subpopulation of spines suggests that individual spines contain a discrete mix of ion channels. In some spines it may be imperative that VDCCs are colocalized with receptors that are incapable of mediating Ca^{2+} influx. In other spines, where N-type VDCCs colocalize with either ligand or voltage-gated calcium channels, they may be important amplifiers of Ca^{2+} influx. Presumably, in those spines lacking N-type VDCCs, Ca^{2+} influx occurs through NMDA (Burnashev et al., 1992), or other excitatory receptors (Regehr et al., 1989; Hume et al., 1991; Seguela et al., 1993), or other subtypes of VDCCs. Plausibly, differences in the complexion of ion channels in individual spines endow the neuron with a heterogeneity of postsynaptic sites. Such heterogeneity could be a means of fine tuning the responses to excitatory synaptic input, particularly if the spine membrane composition is dynamic. It is tempting to speculate that the addition and subtraction of various classes of VDCCs may be an essential correlate of synaptic plasticity.

The presence of VDCCs on dendritic spines confirms many predictions of current biophysical models of information processing in dendrites (Gamble and Koch, 1987; Segev and Rall, 1988; Jaslove, 1992). Several studies have shown rises in Ca^{2+} in CA1 dendrites through activation of NMDA receptors (Connor et al., 1988; Regehr and Tank, 1990), proteins implicated in learning and memory (Bliss and Collingridge, 1993). However, non-NMDA receptor mechanisms of Ca^{2+} entry, including those involving VDCCs (Grover and Teyler, 1990; Hume et al., 1991), occur at normal and potentiated synapses in CA1. Our data are consistent with these studies by showing that VDCCs reside on spines where they are poised for a pivotal role in synaptic plasticity. Under appropriate conditions of excitatory input, activation of VDCCs by depolarization would serve to amplify Ca^{2+} influx, particularly in spines where VDCCs and glutamate receptors are colocalized. The precise contribution of VDCCs to spine events will depend on both channel density and spine geometry (Wickens, 1988: Holmes, 1990; Koch and Zador, 1993). On spines with low neck resistances, VDCCs could facilitate Ca^{2+} signaling between adjacent spines and thus may contribute to the cooperativity underlying long-term potentiation (LTP) (McNaughton, 1982; Bliss and Collingridge, 1993). The targeting of N-type VDCCs to a subset of spines is a novel mechanism for the selective modification of Ca^{2+} levels and is consistent with the emerging view that spines may reg-

ulate Ca^{2+} independently from their parent dendrites and from one another (Guthrie et al., 1991; Muller and Connor, 1991).

References

Andersen P (1986) Factors influencing the efficiency of dendritic synapses on hippocampal pyramidal cells. Neurosci Res 3:521–530.

Andersen P, Silfrenius H, Sundberg S, Sveen O (1980) A comparison of distal and proximal dendritic synapses on CA1 pyramids in guinea-pig hippocampal slices *in vitro*. J Physiol (Lond) 307:273–299.

Andrews SB, Leapman RD, Landis DM, Reese TS (1988) Activity-dependent accumulation of calcium in Purkinje cell dendritic spines. Proc Natl Acad Sci USA 85:1682–1685.

Augustine GJ, Neher E (1992) Neuronal Ca^{2+} signalling takes the local route. Curr Opin Neurobiol 2:302–307.

Augustine GJ, Charlton MP, Smith SJ (1987) Calcium action in synaptic transmitter release. Annu Rev Neurosci 10:633–693.

Bading H, Ginty DD, Greenberg ME (1993) Regulation of gene expression in hippocampal neurons by distinct calcium signalling pathways. Science 260:181–186.

Blaxter T, Carlen PL, Niesen CE (1989) Pharmacological and anatomical separation of calcium currents in rat dentate granule neurones *in vitro*. J Physiol (Lond) 412:93–112.

Bliss TVP, Collingridge GL (1993) A synaptic model of memory: long-term potentiation in the hippocampus. Nature 361:31–39.

Burnashev N, Schoepfer R, Monyer RF, Ruppersberg JP, Gunther W, Seeburg PH, Sakmann B (1992) Control by asparagine residues of calcium permeability and magnesium blockade in the NMDA receptor. Science 257:1415–1419.

Choi DW (1988) Glutamate toxicity and diseases of the nervous system. Neuron 1:623–634.

Cohen MW, Jones OT, Angelides KJ (1991) Distribution of Ca^{2+} channels on frog motor nerve terminals revealed by fluorescent ω-conotoxin. J Neurosci 11:1032–1039.

Connor JA, Wadman WJ, Hockberger P, Wong RKS (1988) Sustained dendritic gradients of Ca^{2+} induced by excitatory amino acids in CA1 hippocampal neurons. Science 240:649–653.

Craig AW, Blackstone CD, Huganir RL, Banker G (1993) The distribution of glutamate receptors in cultured rat hippocampal neurons: postsynaptic clustering of AMPA-selective subunits. Neuron 10:1055–1068.

Dotti CG, Simons K (1990) Polarized sorting of viral glycoproteins to the axon and dendrites of hippocampal neurons in culture. Cell 62:63–72.

Fifkova E, Morales M (1992) Aging and the neurocytoskeleton. Exp Gerontol 27:125–136.

Fisher RE, Gray R, Johnston D (1990) Properties and distribution of single voltage-gated calcium channels in adult hippocampal neurons. J Neurophysiol 64:91–104.

Gamble E, Koch C (1987) The dynamics of free calcium in dendritic spines in response to repetitive synaptic input. Science 236:1311–1315.

Gibson GE, Peterson C (1987) Calcium and the aging nervous system. Neurobiol Aging 8:329–343.

Glossmann H, Striessnig J (1990) Molecular properties of calcium channels. Rev Physiol Biochem Pharmacol 114:1–105.

Grover LM, Teyler TJ (1990) Two components of long-term potentiation induced by different patterns of afferent activation. Nature 347:477–479.

Guthrie PB, Segal M, Kater SB (1991) Independent regulation of calcium revealed by imaging dendritic spines. Nature 354:76–80.

Harris KM, Stevens JK (1989) Dendritic spines of CA1 pyramidal cells in the rat hippocampus: serial electron microscopy with reference to their biophysical characteristics. J Neurosci 9:2982–2997.

Harris KM, Jensen FE, Tsao B (1992) Three-dimensional structure of dendritic spines and synapses in rat hippocampus (CA1) at postnatal day 15 and adult ages: implications for the maturation of synaptic physiology and long-term potentiation. J Neurosci 12:2685–2705.

Holmes WR (1990) Is the function of dendritic spines to concentrate calcium? Brain Res 519:338–342.

Horne AL, Kemp JA (1991) The effect of ω-conotoxin GVIA on synaptic transmission within the nucleus accumbens and hippocampus of the rat *in vitro*. Br J Pharmacol 103:1733–1739.

Hosokawa T, Bliss TVP, Fine A (1992) Persistence of individual spines in living brain slices. Neuroreport 3:477–480.

Hounsgaard J, Mittgaard J (1989) Dendrite processing in more ways than one. Trends Neurosci 12:313–315.

Hume RI, Dingledine R, Heinemann SF (1991) Identification of a site in glutamate receptor subunits that controls calcium permeability. Science 253:1028–1031.

Jaslove SW (1992) The integrative properties of spiny distal dendrites. Neuroscience 47:495–519.

Jones OT, Kunze DL, Angelides KJ (1989) Localization and mobility of ω-conotoxin-sensitive Ca^{2+} channels in hippocampal CA1 neurons. Science 244:1189–1193.

Kater SB, Mills LR (1991) Regulation of growth cone behavior by calcium. J Neurosci 11:891–899.

Katz B (1969) The release of neural transmitter substances. Liverpool: Liverpool UP.

Kerr LM, Filloux F, Olivera BM, Jackson H, Wamsley JK (1988) Autoradiographic localization of calcium channels with [^{125}I]ω-conotoxin in rat brain. Eur J Pharmacol 146:181–183.

Koch C, Zador A (1993) The function of dendritic spines: devices subserving biochemical rather than electrical compartmentalization. J Neurosci 13:413–422.

Koch C, Zador A, Brown TH (1992) Dendritic spines: convergence of theory and experiment. Science 256:973–974.

Komura H, Rakic P (1992) Selective role of N-type calcium channels in neuronal migration. Science 257:806–809.

Konnerth A, Dreesen J, Augustine GJ (1992) Brief dendritic calcium signals initiate long-lasting synaptic depression in cerebellar Purkinje cells. Proc Natl Acad Sci USA 89:7051–7055.

Kullmann DM, Perkel DJ, Manabe T, Nicoll RA (1992) Ca^{2+} entry via postsynaptic voltage-sensitive Ca^{2+} channels can transiently potentiate excitatory synaptic transmission in the hippocampus. Neuron 9:1175–1183.

Lin CH, Forscher P (1993) Cytoskeletal remodelling during growth cone–target interactions. J Cell Biol 121:1369–1383.

Lipscombe D, Madison DV, Poenie M, Reuter H, Tsien RY, Tsien RW (1988) Spatial distribution of calcium channels and cytosolic calcium transients in growth cones and cell bodies of sympathetic neurons. Proc Natl Acad Sci USA 85:2398–2402.

Llinás RR (1988) The intrinsic electrophysiological properties of mammalian neurons: insights into central nervous system function. Science 242:1654–1664.

Llinás R, Sugimori M (1979) Calcium conductances in purkinje cell dendrites: their role in development and integration. Prog Brain Res 51:323–334.

Llinás R, Sugimori M (1980) Electrophysiological properties of *in vitro* Purkinje cell dendrites in mammalian cerebellar slices. J Physiol (Lond) 305:197–213.

Lynch G, Larson J, Kelso S, Barrionuevo G, Schottler F (1983) Intracellular inductions of EGTA block induction of hippocampal LTP. Nature 305:719–721.

Malenka RC, Kauer JA, Zucker RS, Nicoll RA (1988) Postsynaptic calcium is sufficient for potentiation of hippocampal synaptic transmission. Science 243:81–84.

McNaughton BL (1982) Long-term synaptic enhancement and short-term potentiation in rat fascia dentata act through different mechanisms. J Physiol (Lond) 324:249–262.

Miller RJ (1992) Voltage-sensitive Ca^{2+} channels. J Biol Chem 267: 1403–1406.

Mills LR (1994) Dynamic intracellular calcium compartments: confocal microscopy using fluo-3 in cells and organelles. In: Three-dimensional confocal microscopy (Stevens JKS, Mills LR, Trogadis JE, eds), in press. San Diego: Academic.

Mills LR, Nurse CA (1993) Chronic hypoxia *in vitro* increases the volume of dissociated carotid body chemoreceptors. Neuroreport 4:619–626.

Mills LR, Niesen X, Kerr R (1994) Confocal imaging of living neurons and organelles. In: Three-dimensional confocal microscopy (Stevens JKS, Mills LR, Trogadis JE, eds), in press. San Diego: Academic.

Mintz IM, Adams ME, Bean BP (1992) P-type calcium channels in rat central and peripheral neurons. Neuron 9:85–95.

Miyakawa H, Ross WN, Jaffe D, Callaway JC, Lasser-Ross N, Lisman JE, Johnston D (1992) Synaptically activated increases in Ca^{2+} concentration in hippocampal CA1 pyramidal cells are primarily due to voltage-gated Ca^{2+} channels. Neuron 9:1163–1173.

Muller W, Connor JA (1991) Dendritic spines as individual neuronal compartments for synaptic Ca^{2+} responses. Nature 354:73–76.

Olivera BM, Rivier J, Scott JK, Hillyard DR, Cruz LJ (1991) Conotoxins. J Biol Chem 266:22067–22070.

Perkel DH, Perkel DJ (1985) Dendritic spines: role of active membrane in modulating synaptic efficiency. Brain Res 325:331–335.

Peters A, Palay SL, Webster HdeF (1991) The fine structure of the nervous system, 3d ed. London: Oxford UP.

Regan LJ, Sah DWY, Bean BP (1991) Ca^{2+} channels in rat central and peripheral neurons: high-threshold current resistant to dihydropyridine blockers and ω-conotoxin. Neuron 6:269–280.

Regehr WG, Tank DW (1990) Postsynaptic NMDA receptor-mediated calcium accumulation in hippocampal CA1 pyramidal cell dendrites. Nature 345:807–810.

Regehr WG, Tank DW (1992) Calcium concentration dynamics produced by synaptic activation of CA1 hippocampal pyramidal cells. J Neurosci 12:4202–4223.

Regehr WG, Connor JA, Tank DW (1989) Optical imaging of calcium accumulation in hippocampal pyramidal cells during synaptic activation. Nature 341:533–536.

Rigaut JP, Vassy J (1991) High-resolution three-dimensional images from confocal scanning laser microscopy: quantitative study and mathematical correction of the effects of bleaching and fluorescence attenuation in depth. Anal Quant Cytol Histol 13:223–232.

Robitaille R, Adler EM, Charlton MP (1990) Strategic location of calcium channels at transmitter releases sites of frog neuromuscular synapses. Neuron 5:773–779.

Rodriguez-Boulan E, Powell SK (1992) Polarity of epithelial and neuronal cells. Annu Rev Cell Biol 8:395–427.

Sala F, Hernandez-Cruz A (1990) Calcium diffusion in a spherical neuron. Relevance of buffering properties. Biophys J 57:313–324.

Schwartzkroin PA, Slawsky M (1977) Probable calcium spikes in hippocampal neurons. Brain Res 135:157–161.

Segev I, Rall W (1988) Computational study of an excitable dendritic spine. J Neurophysiol 60:499–523.

Seguela P, Wadiche J, Dineley-Miller K, Dani JA, Patrick JW (1993) Molecular cloning, functional properties, and distribution of rat brain alpha 7: a nicotinic cation channel highly permeable to calcium. J Neurosci 13:596–604.

Seubert P, Larson J, Oliver M, Jung MW, Baudry M, Lynch G (1988) Stimulation of NMDA receptors produces proteolysis of brain spectrin in hippocampal slices. Brain Res 460:189–195.

Sheng M, Greenberg ME (1990) The regulation and function of c-fos and other immediate early genes in the nervous system. Neuron 4:477–485.

Shepherd GM, Brayton RK, Miller JF, Segev I, Rinzel J, Rall W (1985) Signal enhancement in distal cortical dendrites by means of interactions between active dendritic spines. Proc Natl Acad Sci USA 82: 2192–2195.

Shepherd GM, Woolf TB, Carnevale NT (1990) Comparisons between active properties of distal dendritic branches and spines: implications for neuronal computations. J Cognit Neurosci 1:273–286.

Sher E, Clementi E (1991) ω-conotoxin-sensitive voltage-operated calcium channels in vertebrate cells. Neuroscience 42:301–307.

Silver RA, Lamb AG, Bolsover SR (1990) Calcium hotspots caused by L-channel clustering promote morphological changes in neuronal growth cones. Nature 343:751–754.

Srinivasan Y, Elmer L, Davis J, Bennett V, Angelides KJ (1988) Ankyrin and spectrin associate with voltage-dependent sodium channels in brain. Nature 333:177–180.

Stevens JKS, Trogadis JE, Mills LR, Leitao C (1990) Three-dimensional volume investigation of serial confocal data sets. Micro 90: 375–380.

Takemura M, Kiyama H, Tohyama M, Wada H (1988) Autoradiographic visualization in rat brain of receptors for ω-conotoxin GVIA, a newly discovered calcium antagonist. Brain Res 451:386–389.

Turner TJ, Adams ME, Dunlap K (1992) Calcium channels coupled to glutamate release identified by omega-AgaIVA. Science 258:310–313.

Westenbroek RE, Ahlijanian MK, Catterall WA (1990) Clustering of L-type Ca^{2+} channels at the base of major dendrites in the hippocampal pyramidal neurons. Nature 347:281–284.

Westenbroek R, Hell JW, Warner C, Dubel SJ, Snutch TP, Catterall WA (1992) Biochemical properties and subcellular distribution of an N-type calcium channel α1 subunit. Neuron 9:1099–1115.

Wickens J (1988) Electrically coupled but chemically isolated synapses: dendritic spines and calcium in a rule for synaptic modification. Prog Neurobiol 31:507–528.

Witcher DR, De Waard M, Sakamoto J, Franzini-Armstrong C, Pragnell M, Kahl SD, Campbell KP (1993) Subunit identification and reconstitution of the N-type Ca^{2+} channel complex purified from brain. Science 261:486–489.

Wong RKS, Stewart M (1992) Different firing patterns generated in dendrites and somata of CA1 pyramidal neurones in guinea-pig hippocampus. J Physiol (Lond) 457:675–687.

Wong RKS, Prince DA, Basbaum A (1979) Intradendritic recordings from hippocampal neurons. Proc Natl Acad Sci USA 76:986–990.